F. CLAEYSSENS
G.M. FUGE
N.L. ALLAN
P.W. MAY
S.R.J. PEARCE
M.N.R. ASHFOLD✉

Phosphorus carbide thin films: experiment and theory

School of Chemistry, University of Bristol, Bristol BS8 1TS, UK

ABSTRACT The recent finding that radio frequency plasma activation of CH_4/PH_3 gas mixtures [7] could lead to films with P : C ratios ≤ 3 (which also contain $\sim 10\%$ hydrogen, distributed evenly throughout the bulk) has served to trigger further research into new 'amorphous phosphorus carbide' materials. New theoretical and experimental results relating to these materials are presented here. The electronic structure and stability of different crystalline phosphorus carbide P_xC_y phases have been studied using first-principles density-functional theory methods. Calculations have been carried out for both P_4C_3 and PC and a range of the more likely periodic structures examined. The lowest energy pseudocubic P_4C_3 and GaSe PC phases have been further investigated as templates to discover the stability and the electronic and structural properties of these phosphorus carbide materials. Recent experimental studies have involved use of pulsed laser ablation (PLA) methods to produce hydrogen-free phosphorus carbide thin films. Mechanically hard, electrically conducting diamond-like carbon films containing $0-\sim 26$ at. % P have been deposited on both Si and quartz substrates by 193 nm PLA of graphite/phosphorus targets (containing varying percentages of phosphorus), at a range of substrate temperatures ($T_{sub} = 25–400\,°C$), in vacuum, and analysed via laser Raman and X-ray photoelectron spectroscopy.

PACS 68.55.Jk; 71.15.Nc; 81.15.Fg

1 Introduction

The past few years have witnessed major research efforts into binary nitrides. Carbon nitride (C_3N_4) has attracted particular interest, following theoretical predictions that it should exhibit outstanding physical properties, e.g., hardness values comparable to diamond, combined with high toughness [1], and excellent tribological, chemical, and electrical properties. Unfortunately, preparation of crystalline carbon nitride has proven to be extremely challenging and only small amounts of crystalline material have been synthesised to date [2]. Most physical processes used for carbon nitride deposition, e.g., pulsed laser ablation (PLA) [3], cathodic arc

✉ Fax: +44-117/925-1295, E-mail: Mike.Ashfold@bris.ac.uk

deposition [4] and chemical vapour deposition (CVD) [5], have yielded amorphous films containing low (1–10%) percentages of nitrogen. Nitrogen incorporation into the carbon lattice is seemingly very difficult, although exciting synthetic routes toward graphite-like C_3N_4 materials have been recently developed [6].

In contrast to the current experimental impasse in producing either amorphous or crystalline carbon nitride with a high nitrogen content, amorphous thin films of the phosphorus-containing analogue with a wide range of P : C compositions (up to a ratio of 3 : 1) have been produced via capacitively coupled radio frequency (rf) plasma deposition from PH_3/CH_4 gas mixtures [7]. These films also have a small ($\sim 10\%$) hydrogen content, from the gas mixture, and are prone to oxidation, as revealed by secondary ion mass spectrometry (SIMS) and X-ray photoelectron spectroscopy (XPS). UV-VIS spectroscopy reveals a sharp absorption threshold at ~ 2.7 eV in the case of films with small P : C ratios, which shifts progressively to ~ 2 eV as the phosphorus content increases (to P : C ratios ~ 3). These findings have encouraged a number of experimental and theoretical studies of phosphorus carbide thin films. The theoretical studies reported here concentrate on aspects of the structure, bonding and electronic structure of crystalline phosphorus carbides [8, 9], while our recent experimental studies have focused on the production of hydrogen-free phosphorus carbide thin films via PLA methods and their subsequent characterisation [10].

2 Theory

Crystalline structures with stoichiometries P_4C_3 and PC have been investigated using plane-wave density-functional theory (DFT) calculations in the generalised gradient approximation (GGA) as implemented in the CASTEP code [11] with the exchange-correlation functional due to Perdew and Wang [12]. Only valence electrons are considered throughout, with the core electrons replaced by the ultra-soft Vanderbilt potentials [13]. We have checked to ensure that the results are well converged with respect to the real space grid, Brillouin zone sampling and basis set size.

These investigations have identified the pseudocubic form of P_4C_3 and the GaSe form of PC – both shown in Fig. 1 – as the most stable crystalline structures. These results ac-
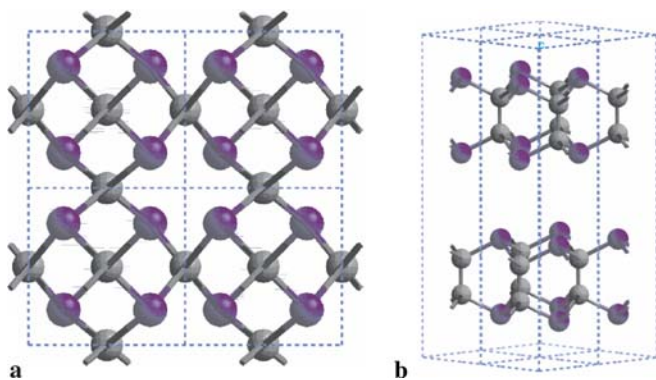
FIGURE 1 Calculated structures for the **a** P_4C_3 and **b** PC stoichiometries. The *lighter* and *darker grey spheres* represent the carbon/phosphorus atoms, respectively, while the *dashed lines* depict the unit cell boundaries

	P_4C_3	PC
Space group	P$\bar{4}$3m(215)	$P3m1$(156)
Volume/formula unit (Å^3)	70.45	24.27
Band gap (eV)	0.00	1.41
Bulk modulus (GPa)	156	64
Cohesive energy (eV)	-5.09	-5.47
Energy of formation (eV/atom)	0.28	0.27
Antisite defect (eV)	1.34	1.87

TABLE 1 Properties of the calculated minimum energy crystalline structures for the stoichiometries P_4C_3 and PC

cord with results published by other groups [14, 15]. Table 1 summarises calculated properties of these two phases. In both structures the carbon atoms are four-fold coordinate, while the phosphorus atoms are three-fold coordinate. In both there is a sp^3-bonded network, which is three-dimensional for P_4C_3 but two-dimensional for the PC stoichiometry. Additionally, there are C−C bonds in the GaSe PC structure but not in the pseudocubic P_4C_3 structure.

While the GaSe structure is also the lowest energy structure for CN (1 : 1 stoichiometry), a comparison between C_3N_4 and P_4C_3 is striking. For C_3N_4, the cubic, α- and β-C_3N_4 structures are each more stable than the pseudocubic. This reversal of stability is linked to differences in the CPC (CNC) bond angles between the different structures. These angles are all considerably larger (typically between 110 and 115°) in the α-, β-, and cubic phases than those in the pseudocubic, all of which are ≈ 104°, closer to the 99° bond angle adopted in, for example, P(CH$_3$)$_3$. This accords with the known molecular chemistries of N and P, where P shows a greater preference for tetrahedral coordination [16]. The CPC angle in the GaSe structure adopted by PC is ≈ 101°, which is close to the bond angle for tetrahedral coordination preferred by phosphorus. By comparison, the CNC angle in the corresponding GaSe CN structure is ≈ 109°.

We have calculated the band structure for the P_4C_3 and PC structures. In the GGA approach, the P_4C_3 structure was calculated to be metallic (no band gap), while the PC structure is an insulator with a direct band gap of 1.41 eV. DFT calculations are notorious for underestimating the band gap, so the reported values should be considered as lower limits for the respective band gaps [17]. The cohesive energy of P_4C_3 is lower than that of PC. The energy of formation of these two structures has also been estimated using the calculated energies of elemental carbon (diamond structure) and phosphorus (black phosphorus). These are both slightly positive but, as with diamond itself, the calculated energy difference is not sufficient to preclude formation of the proposed structures via a kinetically controlled pathway. The bulk moduli are calculated to be 156 and 64 GPa for the P_4C_3 and PC structures, respectively, indicating that the layered, PC structure is less hard than the 3-D pseudocubic P_4C_3 structure. The energies of antisite defects have been calculated also, for both structures, by swapping a C and P atom in large supercells ($2 \times 2 \times 2$

for P_4C_3 and $2 \times 2 \times 1$ for PC) and optimising the resulting cells. These defect energies provide an indication of the ease of amorphisation of the respective structures. For comparison, the calculated antisite defect energies in SiC are much higher (∼ 9 eV) [18].

3   Experimental

P containing DLC (henceforth P-DLC) films were prepared by PLA of phosphorus/carbon targets and deposition on both n-type single-crystal (100) Si and quartz substrates (∼ 1 cm^2 in area) at a range of substrate temperatures ($25 \leq T_{sub} \leq 400$ °C). Targets were prepared from intimately mixed samples of graphite and red phosphorus powder containing, respectively, 10%, 20%, 30% and 50% by weight P. Each was prepared as a 52-mm-diameter disk using a hydraulic press with maximum force of 560 kN and subsequently polished to obtain a smooth, flat surface. The chosen target was mounted on a rotation stage within a stainless steel chamber evacuated to ∼ 10^{-6} Torr. The output of an ArF (193-nm) excimer laser (Lambda-Physik, Compex 201, 10 Hz repetition rate) was focused (450 mm f.l. fused silica lens) onto the target; the focal spot size on the target was ∼ 1 mm^2, thus yielding incident fluences, F, in the range 4–12 J cm^{-2}. The substrate was mounted so that its front face was perpendicular to the target surface normal and 80 mm from the focal spot, on a purpose-designed holder that was itself positioned immediately in front of a compact 15-W light-bulb heater that allowed deposition at any user-selected $T_{sub} \leq 400$ °C [10].

The resulting P-DLC films were analysed by laser Raman spectroscopy (LRS) employing a Renishaw 2000 system and an excitation wavelength of 514.5 nm, by XPS (Fisons Instruments VG Escascope, Mg K_α (1253.6 eV) source, analyser energy resolution of ∼ 0.9 eV) and by scanning electron microscopy (JEOL JSM 5600 LV scanning electron microscope). Spectroscopic ellipsometry was performed on films deposited on Si (J.A. Woollam VASE ellipsometer) at five incident angles between 55 and 75°, yielding values for Δ and Ψ over the spectral range of 200–1000 nm. Film optical constants (n, k) and the thickness were derived using a model of amorphous semiconductor on 0.5-mm-thick crystalline Si, with the semiconductor layer described using the Tauc–Lorentz model [19].

The P-DLC films exhibited a smooth, apparently featureless surface morphology save for a number of randomly dispersed micron-size particulates, which we assume to be crystallites transferred directly from the target surface as a re-
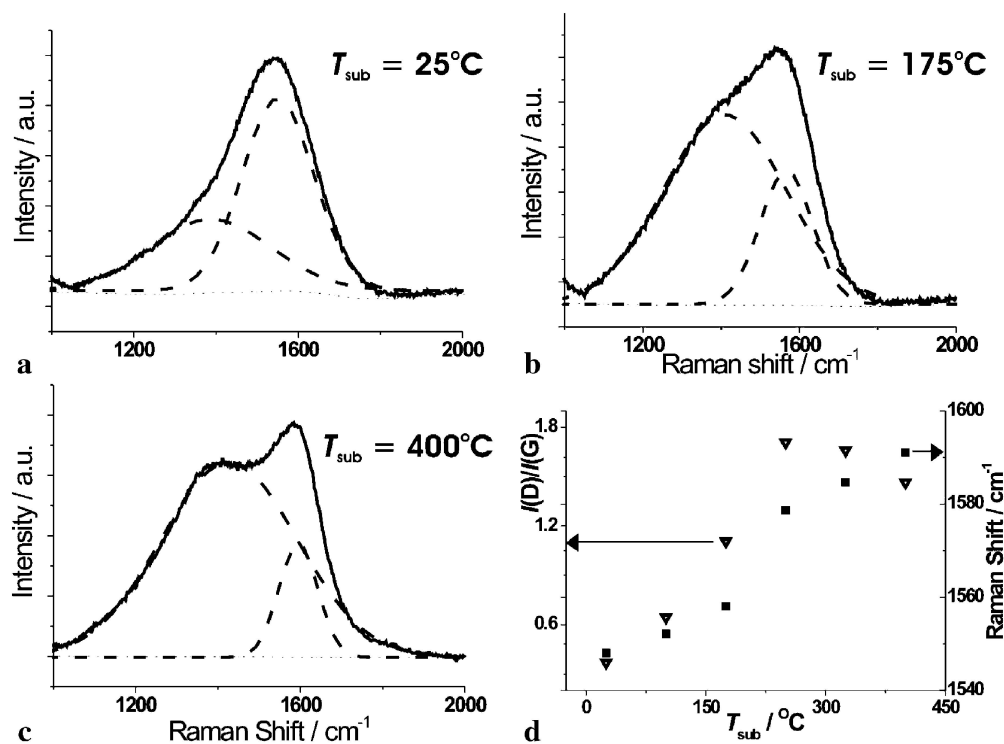
FIGURE 2 Details from the 1000–2000 cm^{-1} regions of Raman spectra (514.5-nm excitation) of P-DLC films grown on n-type Si(100) substrates by PLA of a target comprising 10% P in C (by weight) in vacuum at $T_{sub} = 25\,^{\circ}$C (**a**), 175 $^{\circ}$C (**b**) and 400 $^{\circ}$C (**c**). Each has been fitted in terms of two independent Gaussian functions (*long dashed curves*), while the *short dashed line* at $y \sim 0$ shows the residuals of the fit. **d** T_{sub} dependence of the $I(D)/I(G)$ ratio deduced from such deconvolutions, and the G_{max}

sult of explosive melting of the target surface [20]. The deposited P-DLC film thickness was observed to increase from ~ 30 nm to ~ 50 nm (20-min depositions, at $T_{sub} = 25\,^{\circ}$C) as F was increased from 4 to 12 J cm^{-2} but to decrease with increasing T_{sub}.

Figure 2 presents the results of LRS investigations of P-DLC films deposited on n-type Si(100) substrates. Figure 2a, b, and c illustrate the T_{sub} dependence of the broad feature present in the range 1000–2000 cm^{-1}, which we deconvolute (using Gaussian functions) into contributions associated with the D and G phonon modes of graphite [21]. The wavenumbers of the G and D band maxima (G_{max} and D_{max}) and the ratio of these two peak intensities, $I(D)/I(G)$, offer insight into the nature of the bonding (e.g., degree of graphitisation) in the film. As found previously in the case of N additions [22–26], the addition of dopant atoms (here P) causes a marked increase in the room temperature $I(D)/I(G)$ ratio compared to that found for a pure DLC film deposited under otherwise identical conditions – an observation attributed to increased formation of nanocrystalline graphite and, possibly, fullerene-like structures in the matrix [21]. Both G_{max} and D_{max} are seen to shift to a higher wavenumber with increasing T_{sub}. The $I(D)/I(G)$ ratio also increases with T_{sub} but shows a higher room temperature value and maximises at somewhat lower T_{sub} than found for pure DLC films grown under otherwise identical conditions. Figure 2d summarises the trends with T_{sub}, which mirror those found previously in the case of N doped DLC films [22]. The observed T_{sub} dependences of G_{max}, D_{max} and the $I(D)/I(G)$ ratio are consistent with a shift from amorphous to nanocrystalline film growth [21]. Increasing T_{sub} from 25 $^{\circ}$C to 400 $^{\circ}$C also leads to a marked reduction in the FWHM of the G peak (from ~ 200 cm^{-1} to ~ 100 cm^{-1}), suggesting that increasing T_{sub} aids the structural ordering of the graphitic component.

Figure 3 compares the 200–1000 cm^{-1} region of the Raman spectra of a P-DLC film deposited at $T_{sub} = 25\,^{\circ}$C following PLA of a 50% P in C target, in vacuum, with the corresponding spectral regions measured from a sample of pure red phosphorus, a thin film of phosphorus deposited on a Si substrate by PLD, and of a bare Si substrate. The features evident in the range 320–490 cm^{-1} confirm the presence of P in the deposited film [27], but the spectra clearly differ in significant detail. The spectrum of the P-DLC film lacks the sharp peak at ~ 350 cm^{-1} (generally attributed to P$_9$ cages [28]), and the maximum of the feature has shifted to a higher wavenumber
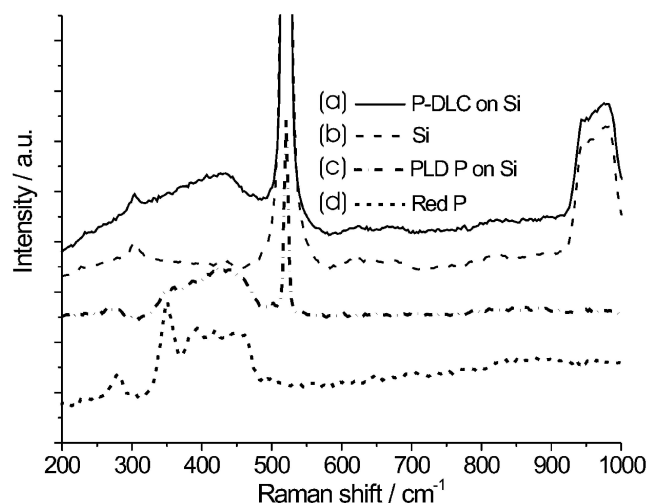

FIGURE 3 Details of the 200–1000 cm^{-1} regions of Raman spectra (514.5-nm excitation) of (**a**) a P-DLC film deposited on Si at $T_{sub} = 25\,^{\circ}$C following PLA of a 50% P in C target in vacuum, (**b**) a bare Si substrate, (**c**) a thin film of phosphorus deposited on Si by PLD and (**d**) a sample of pure red phosphorus. The four spectra have been offset vertically for clarity
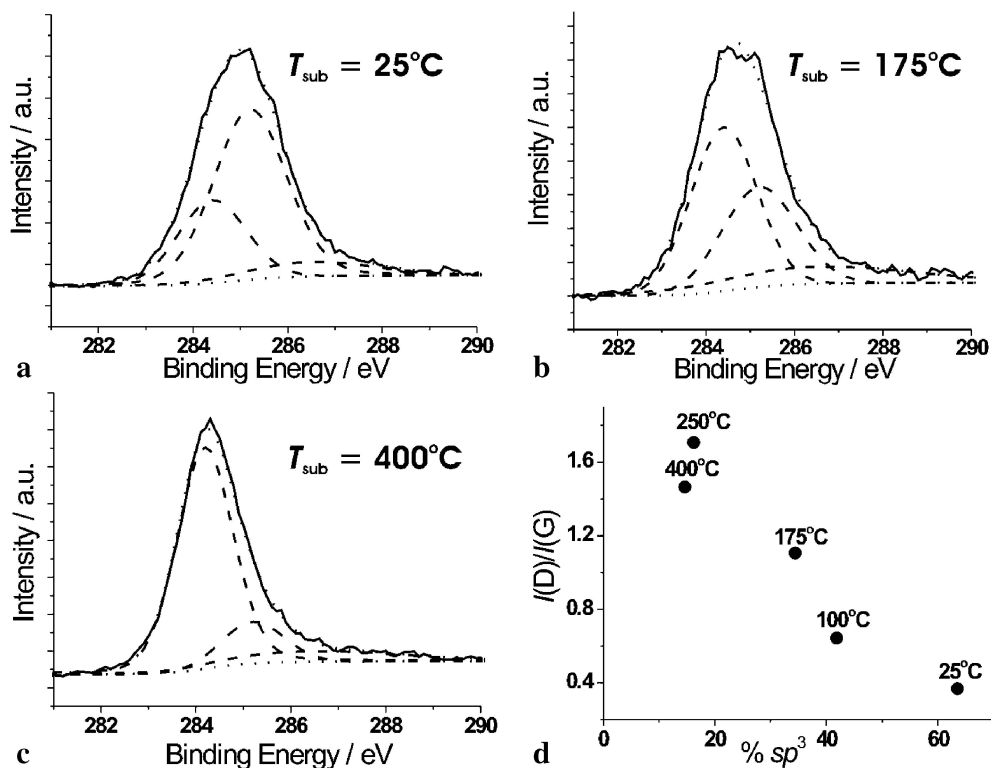
($\sim 430\,cm^{-1}$). This effect is also observed in the spectrum of the phosphorus film grown by PLD (Fig. 3c). The loss of the $350\,cm^{-1}$ peak suggests preferential break-up of larger cages during the PLA process. The absence of any feature $\sim 700\,cm^{-1}$ in the Raman spectrum of the P-DLC film is also noteworthy. This is the region in which C−P bond stretching modes would be expected. This mode should be strongly Raman active; its absence thus suggests minimal C−P bonding in the film.

Figure 4 presents results from XPS analysis of the P-DLC films. The broad (100–600 eV) spectrum shows peaks attributable to P (2s and 2p), C (1s) and O (1s) (from aerial oxidation) [10]. Absolute P/C/O ratios could be determined by comparing the respective peak areas, A_X, weighted by the appropriate atomic sensitivity factors (i.e., P : C : O = $A_P(2p)/0.39 : A_C/0.25 : A_O/0.66$). Such analyses confirmed that the stoichiometry of the P-DLC films followed that of the target. In the case of P-DLC films deposited at $T_{sub} = 25\,°C$, for example, PLA of a 10% P in C target yielded films with a P content of ~ 6.5 at. % (i.e., ~ 15% P by weight), while those grown by PLA of a 50% P in C target were found to contain ~ 18 at. % P (~ 36% P by weight). Increasing T_{sub} caused a decline in P content (e.g., falling to ~ 1.5 at. % in the case of films grown from the 10% P in C target at $T_{sub} = 400\,°C$), as did increasing fluence (e.g., from 25 at. % P to 18 at. % P in the case of films grown from the 50% P in C target as F was increased from ~ 4 to $\sim 12\,J\,cm^{-2}$). These compositional data, and the evident decline in film thickness with increasing T_{sub}, all suggest that P atoms are accommodated less strongly than C during the film growth process.

The first three panels in Fig. 4 show that the detailed shape of the C(1s) peak in the XPS spectrum is sensitive to the actual deposition conditions. As in our previous investigations of CN_x films [22], these line shapes have been deconvoluted in an effort to gain some insight into the ratio of sp^3 to sp^2 bonded carbon in the P-DLC films. Assuming the films contain negligible C−P bonding, we model the C(1s) peak in terms of contributions from C-sp^3, C-sp^2 and C−O bonding only. Such deconvolutions are illustrated in Fig. 4a–c for the respective cases of P-DLC films grown by PLA of a 10% P in C target at three different T_{sub} values. Analysis of the film deposited at room temperature suggests a C-sp^3 content of ~ 64%, which has dropped to ~ 33% for $T_{sub} = 175\,°C$ and to ~ 15% at $T_{sub} = 400\,°C$. These percentages correspond to C $sp^3 : sp^2$ ratios of ~ 2.3, ~ 0.5 and ~ 0.2, respectively. C-sp^3 content is thus maximised at low T_{sub}. The results summarised in Fig. 2d demonstrate that growth at low T_{sub} also results in the lowest $I(D)/I(G)$ ratios. Both sets of observations are consistent with the recognised evolution from amorphous carbon toward the formation of islands of nanocrystalline graphite as T_{sub} is increased. As Fig. 4d shows, there appears to be an inverse correlation between $I(D)/I(G)$ ratio and C-sp^3 content for films grown at $T_{sub} \leq 250\,°C$, though this breaks down at yet higher T_{sub} values. This breakdown can be understood by noting that the $I(D)/I(G)$ vs. T_{sub} plot maximizes at $\sim 325\,°C$. Such trends have been observed, and explained, previously. Above this temperature, the measured $I(D)/I(G)$ ratio is found to vary inversely with the sp^2 cluster size (L_a) [29] – consistent with the turnover at the highest T_{sub} value shown in Fig. 4d.

4 Conclusions

We have presented experimental and theoretical results relating to phosphorus carbide thin films and bulk phases. There is still much to be done, in particular to increase

the crystallinity of the compounds (e.g., by ablation of P targets under a liquid phase and/or by more traditional high-temperature, high-pressure synthetic routes), which would enable much better future contact between theory and experiment. It is hoped that our work will serve to stimulate a wide-ranging experimental exploration of binary phosphorus-carbon compounds.

REFERENCES

1 D.M. Teter, R.J. Hemley: Science **271**, 53 (1996), and references therein
2 C.M. Niu, Y.Z. Lu, C.M. Lieber: Science **261**, 334 (1993)
3 A.A. Voevodin, J.G. Jones, J.S. Zabinski, Z. Czigany, L. Hultman: J. Appl. Phys. **92**, 4980 (2002)
4 Z.M. Zhou, L.F. Xia: J. Phys. D: Appl. Phys. **35**, 1991 (2002)
5 C. Popov, M.F. Plass, R. Kassing, W. Kulisch: Thin Solid Films **356**, 406 (1999)
6 T. Komatsu: J. Mater. Chem. **11**, 799 (2001)
7 S.R.J. Pearce, P.W. May, R.K. Wild, K.R. Hallam, P.J. Heard: Diam. Rel. Mater. **11**, 1041 (2002)
8 F. Claeyssens, N.L. Allan, P.W. May, P. Ordejon, J.P. Oliva: Chem. Commun. **21**, 2494 (2002)
9 F. Claeyssens, J.M. Oliva, P.W. May, N.L. Allan: Int. J. Quantum Chem. **95**, 546 (2003)
10 G.M. Fuge, P.W. May, K.N. Rosser, S.R.J. Pearce, M.N.R. Ashfold: Diam. Rel. Mater. (in press)
11 CASTEP 4.2 academic version, licensed under the UKCP-MSI Agreement, 1999; Rev. Mod. Phys **64**, 1045 (1992)
12 J.P. Perdew, Y. Wang: Phys. Rev. B **45**, 13 244 (1992)
13 D. Vanderbilt: Phys. Rev. B **41**, 7892 (1990)
14 A.T.L. Lim, J.C. Zheng, Y.P. Feng: Int. J. Mod. Phys. B **16**, 1101 (2002)
15 J.C. Zheng, M.C. Payne, Y.P. Feng, A.T.L. Lim: Phys. Rev. B **67**, 153 105 (2003)
16 N.N. Greenwood, A. Earnshaw: *Chemistry of the Elements* (Butterworth-Heinemann, Oxford 1997)
17 I.N. Remediakis, E. Kaxiras: Phys. Rev. B **59**, 5536 (1999)
18 D.P. Birnie III, W.C. Mackrodt, W.D. Kingery: Adv. Ceram. **23**, 571 (1987)
19 G.E. Jellison Jr., V.I. Merkulov, A.A. Puretzky, D.B. Geohegan, G. Eres, D.H. Lowndes, J.B. Caughman: Thin Solid Films **377**, 68 (2000)
20 M.N.R. Ashfold, F. Claeyssens, G.M. Fuge, S.J. Henley: Chem. Soc. Rev. **33**, 23 (2004), and references therein
21 A.C. Ferrari, J. Robertson: Phys. Rev. B **61**, 14095 (2000), and references therein
22 G.M. Fuge, C.J. Rennick, S.R.J. Pearce, P.W. May, M.N.R. Ashfold: Diam. Rel. Mater. **12**, 1049 (2003)
23 Y.H. Cheng, X.L. Qiao, J.G. Chen, Y.P. Wu, C.S. Xie, Y.Q. Wang, D.S. Xu, S.B. Mo, Y.B. Sun: Diam. Rel. Mater. **11**, 1511 (2002)
24 C.W. Ong, X.-A. Zhao, Y.C. Tsang, C.L. Choy, P.W. Chan: Thin Solid Films **280**, 1 (1996)
25 X.-A. Zhao, C.W. Ong, Y.C. Tsang, K.F. Chan, C.L. Choy, P.W. Chan, R.W.M. Kwok: Thin Solid Films **322**, 245 (1998)
26 M.E. Ramsey, E. Poindexter, J.S. Pelt, J. Marin, S.M. Durbin: Thin Solid Films **360**, 82 (2000)
27 D.J. Olego, J.A. Baumann, M.A. Kuck, R. Schachter, C.G. Michel: Solid State Commun. **52**, 311 (1984)
28 G. Fasol, M. Cardona, W. Hönle, H.G. von Schnering: Solid State Commun. **52**, 307 (1984)
29 F. Tuinstra, J.L. Koenig: J. Chem. Phys. **53**, 1126 (1970)